

## THE FINAL FATES OF ACCRETING SUPERMASSIVE STARS

HIDEYUKI UMEDA<sup>1</sup>, TAKASHI HOSOKAWA<sup>2,3</sup>, KAZUYUKI OMUKAI<sup>4</sup>, NAOKI YOSHIDA<sup>3,5</sup>

*Draft version October 28, 2018*

### ABSTRACT

The formation of supermassive stars (SMSs) via rapid mass accretion and their direct collapse into black holes (BHs) is a promising pathway for sowing seeds of supermassive BHs in the early universe. We calculate the evolution of rapidly accreting SMSs by solving the stellar structure equations including nuclear burning as well as general relativistic (GR) effects up to the onset of the collapse. We find that such SMSs have less concentrated structure than fully-convective counterpart, which is often postulated for non-accreting ones. This effect stabilizes the stars against GR instability even above the classical upper mass limit  $\gtrsim 10^5 M_\odot$  derived for the fully-convective stars. The accreting SMS begins to collapse at the higher mass with the higher accretion rate. The collapse occurs when the nuclear fuel is exhausted only for cases with  $\dot{M} \lesssim 0.1 M_\odot \text{ yr}^{-1}$ . With  $\dot{M} \simeq 0.3 - 1 M_\odot \text{ yr}^{-1}$ , the star becomes GR-unstable during the helium-burning stage at  $M \simeq 2 - 3.5 \times 10^5 M_\odot$ . In an extreme case with  $10 M_\odot \text{ yr}^{-1}$ , the star does not collapse until the mass reaches  $\simeq 8.0 \times 10^5 M_\odot$ , where it is still in the hydrogen-burning stage. We expect that BHs with roughly the same mass will be left behind after the collapse in all the cases.

*Subject headings:* cosmology: theory – early universe – galaxies: formation – stars: formation – accretion – general relativity

### 1. INTRODUCTION

Recent discovery of luminous quasars at  $z > 6$  suggests the existence of black holes with mass exceeding  $10^9 M_\odot$  when the age of the Universe was less than one billion years (e.g., Mortlock et al. 2011; Wu et al. 2015). The formation process of such supermassive black holes (SMBHs) is largely unknown, and poses a serious challenge to the theory of structure formation.

The so-called direct collapse scenario (Bromm & Loeb 2003) provides an attractive pathway for the early BH formation via a peculiar mode of the primordial star formation. This scenario supposes the gravitational collapse of a primordial gas cloud forming a supermassive star with a mass of  $\gtrsim 10^5 M_\odot$ . Specifically, the formation process proceeds in a two-step manner; a very small ( $\ll M_\odot$ ) protostar first forms at the densest part of the cloud, and then grows in mass by rapid accretion from the surrounding envelope (e.g., Latif et al. 2013; Inayoshi et al. 2014; Becerra et al. 2015). The accretion rate onto the protostar is expected to be as large as  $\sim 0.1 - 1 M_\odot \text{ yr}^{-1}$ , with which the stellar mass will exceed  $\gtrsim 10^5 M_\odot$  in less than the stellar lifetime. Such a supermassive star, if successfully formed, eventually collapses into a BH either by the core-collapse or by the general relativistic (GR) instability (e.g., Iben 1963; Chandrasekhar 1964). Given the massive remnant BH as a seed, a SMBH with more than  $10^9 M_\odot$  can be assembled through further growth by accretion and/or mergers in less than one billion years

(e.g., Di Matteo et al. 2012).

The size and the internal structure of an accreting protostar (e.g., Omukai & Palla 2003; Ohkubo et al. 2009) and its resulting radiative feedback effect, which potentially terminates the mass accretion (e.g., McKee & Tan 2008; Hosokawa et al. 2011, 2016; Stacy et al. 2016), are key ingredients to set the final stellar mass (e.g., Hirano et al. 2015). Recent calculations show that the protostar structure is substantially modified if the accretion rate exceeds a few  $\times 10^{-2} M_\odot \text{ yr}^{-1}$ ; the star inflates to have an extended radius of 10 – 100 AU (e.g., Hosokawa et al. 2012, 2013; Schleicher et al. 2013). Since such a fluffy protostar has low effective temperature and hence very low UV luminosity, the radiative feedback does not disturb the accretion flow at least until the stellar mass exceeds  $\sim 10^5 M_\odot$  as long as continuous and efficient gas accretion ensues.

In this *Letter*, we extend our stellar evolution calculations until the SMSs begin to collapse. Our calculations determine the final mass of the accreting SMSs by incorporating the realistic conditions within the context of the direct collapse scenario. Previous studies show that the GR instability causes the collapse of a non-rotating SMS with  $\gtrsim$  a few  $\times 10^5 M_\odot$  but without considering its evolution under rapid mass accretion (e.g., Osaki 1966; Unno 1971; Fricke 1973; Fuller et al. 1986). We show that gas accretion significantly alters the stellar structure. With a very large accretion rate, a star continues to grow in mass without collapsing by the GR instability until the stellar mass reaches  $\sim 10^6 M_\odot$ . Our calculations show the final fate of such a SMS.

### 2. METHOD AND MODEL

We solve the stellar evolution equations using a modified code developed in Umeda et al. (2009), incorporating the GR effects in the post-Newtonian approximation (Fuller et al. 1986). We adopt a primordial abundance pattern for an initial model with hydrogen and helium

<sup>1</sup> Department of Astronomy, The University of Tokyo, Tokyo 113-0033, Japan

<sup>2</sup> Department of Physics, Kyoto University, Kyoto 606-8502, Japan

<sup>3</sup> Department of Physics and Research Center for the Early Universe, The University of Tokyo, Tokyo 113-0033, Japan

<sup>4</sup> Astronomical Institute, Tohoku University, Sendai 980-8578, Japan

<sup>5</sup> Kavli Institute for the Physics and Mathematics of the Universe, University of Tokyo, Kashiwa, Chiba 277-8583, Japan

TABLE 1  
FINAL STELLAR MASS AND COMPOSITION OF THE INNER CORE

$\dot{M}[M_{\odot}/\text{yr}]$	0.1	0.3	1.0	10
$M_f[M_{\odot}]$	$1.2 \times 10^5$	$1.9 \times 10^5$	$3.5 \times 10^5$	$8.0 \times 10^5$
$Y$ (or $X$ )	0.00	0.99	1.00	(0.51)

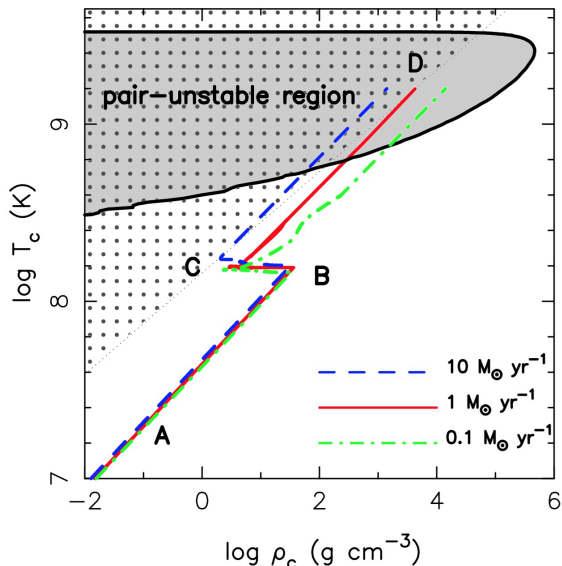


FIG. 1.— The evolution of the central temperature and density for the cases with different accretion rates of  $\dot{M} = 0.1, 1,$  and  $10 M_{\odot} \text{ yr}^{-1}$ . The gray-shaded area denotes the electron-positron pair-unstable region. The star becomes GR-unstable in the dot-shaded area under the assumptions of the  $n = 3$  polytropic structure and primordial composition.

mass fractions  $X = 0.753$  and  $Y = 0.247$ , and the same nuclear reaction networks as in Umeda & Nomoto (2002, 2005) and Umeda et al. (2009). A major difference of the code from that of Hosokawa et al. (2012, 2013) is that no entropy generated at the accretion shock is assumed to be incorporated into the stellar interior. This corresponds to  $\eta = 0$  models in Hosokawa et al. (2013), where  $\eta$  is the fraction of the accretion energy deposited in the stellar interior. However, varying this setting only affects the early evolution for the total stellar mass  $M \lesssim 100 M_{\odot}$ .

We follow the evolution of an accreting protostar with four different rates of  $\dot{M} = 0.1, 0.3, 1,$  and  $10 M_{\odot} \text{ yr}^{-1}$ , starting with a  $10 M_{\odot}$  initial model which has an inflated structure. We first checked that our calculations well reproduce the previous results by Hosokawa et al. (2012, 2013), who study the evolution before the GR effect becomes important. We terminate the calculations when the stellar central temperature reaches  $\log T_c(\text{K}) = 9.2$ , after which the evolutionary timescale is so short that the stellar mass hardly increases thereafter. The final mass and thus the final fate of the star are determined at this epoch.

### 3. RESULTS

In Figure 1 we show the evolution of the central temperature and density for the cases with  $\dot{M} = 0.1, 1$  and  $10 M_{\odot} \text{ yr}^{-1}$ . Although the evolutionary tracks in this figure are quite similar for all the models, there are some differences in the actual evolution, including the cause

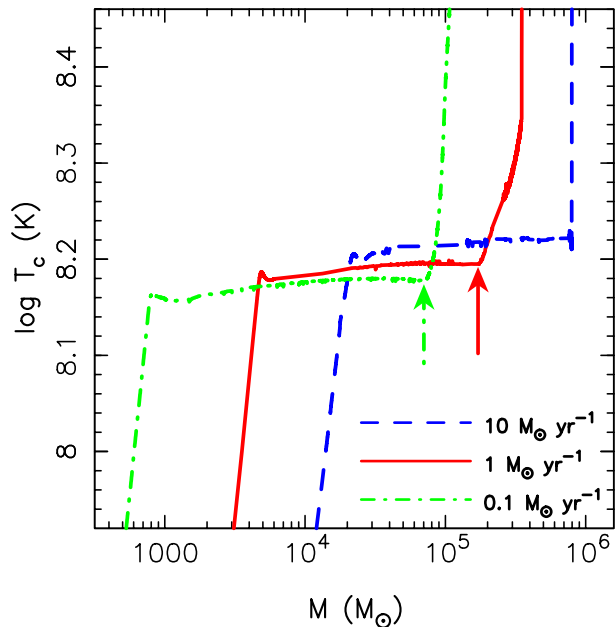


FIG. 2.— The evolution of the central temperature  $T_c$  as the stellar mass increases. Only the values around the stable nuclear burning are shown for clarity. The different lines represent the different accretion rates,  $10 M_{\odot} \text{ yr}^{-1}$  (blue dashed),  $1 M_{\odot} \text{ yr}^{-1}$  (red solid), and  $\dot{M} = 0.1 M_{\odot} \text{ yr}^{-1}$  (green dot-dashed line). The vertical arrows indicate the points where the central hydrogen is exhausted with  $\dot{M} = 0.1$  and  $1 M_{\odot} \text{ yr}^{-1}$ .

of the final collapse, as described below. From A to B in Figure 1, the stellar core contracts monotonically over the Kelvin-Helmholtz timescales until the hydrogen burning via the CNO cycle starts to sustain the star. Although the evolutions from A to B are almost identical with different  $\dot{M}$  values in Figure 1, Figure 2 shows that the stellar mass at point B is larger for higher  $\dot{M}$ . As shown in these figures, the central temperature at point B, i.e., when the hydrogen burning begins, is  $\log T_c(\text{K}) \simeq 8.2$  with only very weak dependence on  $\dot{M}$ . During the hydrogen burning, i.e., from B to C in Figure 1, the central temperature remains almost constant while the density decreases by more than a factor of 10. This is because the central entropy is in general higher for more massive stars, and thus an accreting star evolves toward higher entropy (lower density) regions as its mass increases. After either the exhaustion of nuclear fuel at the center (for the cases with  $0.1 M_{\odot} \text{ yr}^{-1}$ ) or the onset of the GR instability (for 1 and  $10 M_{\odot} \text{ yr}^{-1}$ ), the stellar core contracts again toward D. Figure 2 shows that this occurs at higher stellar mass for higher accretion rate. In all the models, the stars eventually enter the electron-positron pair-unstable region. It is known that stars with  $M \simeq 300 - 1000 M_{\odot}$  collapse directly to form BHs without explosion once entering this region (e.g., Takahashi et al. 2014). Presumably, our SMSs also will follow the same fate (see Section 4).

Table 1 summarizes the stellar masses and mass fractions  $X$  or  $Y$  for the different accretion rates when the central temperature reaches  $\log T_c(\text{K}) = 8.7$ . We here show the mass fractions not at the very center but at the slightly outer part  $M_r = 0.1 M_{\text{core}}$ , where  $M_{\text{core}}$  is the core mass, because the central composition changes relatively fast in the final collapse stage. The central hy-

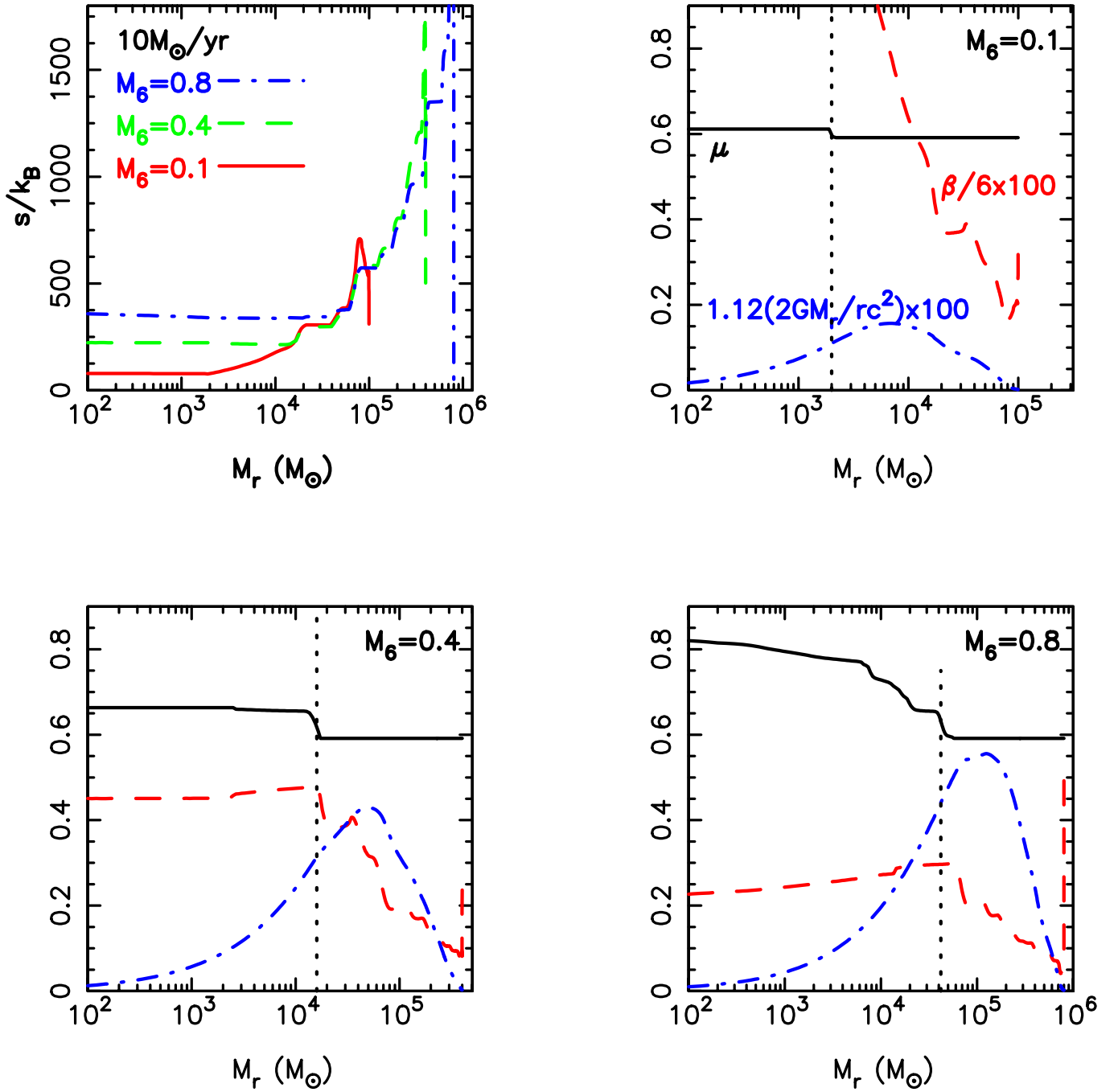


FIG. 3.— The evolution of the stellar interior structure with the accretion rate  $\dot{M} = 10 M_{\odot} \text{ yr}^{-1}$ . The upper left panel shows the evolution of the entropy distribution inside the star. The different lines represent the different epochs when the stellar mass is  $10^5 M_{\odot}$  (red solid),  $4 \times 10^5 M_{\odot}$  (green dashed), and  $8 \times 10^5 M_{\odot}$  (blue dot-solid line). The other panels show the development of the GR instability at the same epochs, at  $M = 10^5 M_{\odot}$  (upper right),  $4 \times 10^5 M_{\odot}$  (lower left), and  $8 \times 10^5 M_{\odot}$  (lower right). In each panel, the radial distributions of  $\beta/6$ ,  $1.12(2GM_r/rc^2)$ , and  $\mu$  are presented with the red dashed, blue dot-solid, and black solid lines, respectively. The former two quantities are multiplied by a factor of 100. The vertical dotted lines indicate the mass coordinates corresponding to the surface of the isentropic core (also see text).

drogen has been exhausted by the onset of the collapse in the cases with  $\dot{M} \leq 1 M_{\odot} \text{ yr}^{-1}$ , for which the values of the helium fraction  $Y$  are described in Table 1. On the other hand, we show the hydrogen mass fraction  $X$  for the model with the highest rate  $\dot{M} = 10 M_{\odot} \text{ yr}^{-1}$ , where the hydrogen still remains at the center.

The GR instability of SMSs has been studied for stellar models with the polytropic equation of state with  $n = 3$

assuming that the entire star is radiation-pressure dominant. For the  $n = 3$  polytropic star, the critical central temperature above which the GR instability occurs can be written as (Shapiro & Teukolsky 1983),

$$T_{\text{crit}} \simeq 2.5 \times 10^7 (0.5/\mu) M_6^{-1} (\text{K}), \quad (1)$$

where  $M_6 \equiv M/10^6 M_{\odot}$  and  $\mu$  is the mean molecular weight. As shown in Figure 2, the central temperature

during the stable hydrogen and helium burning phase is roughly constant at  $\log T_c(\text{K}) \simeq 8.2$  for all the models. For this temperature, the critical mass for the GR instability is given by

$$M_6^{\text{crit}} \simeq 0.16 \times (0.5/\mu), \quad (2)$$

where  $M_6^{\text{crit}}$  is normalized with  $10^6 M_\odot$ . With the mean molecular weight  $\mu \simeq (2X + 3Y/4)^{-1} = 0.59$  for the initial primordial abundance (1.33 for the pure helium matter), the critical mass is  $M_6^{\text{crit}} \simeq 0.14$  (0.06, respectively).

As shown in Table 1, the final mass in our case with  $\dot{M} = 0.1 M_\odot \text{ yr}^{-1}$  is  $M_6 = 0.12$ , smaller than the critical mass estimated above. In fact, the collapse in this case is not triggered by the GR instability. The star just collapses after exhausting the central hydrogen and helium. For  $\dot{M} \gtrsim 0.3 M_\odot \text{ yr}^{-1}$ , on the other hand, the collapse occurs while the nuclear fusion is still in operation, suggesting that the GR instability causes the collapse. The final masses in these cases are, however, again much larger than the critical masses for the polytropic stars given by equation (2).

To understand these differences, we show in Figure 3 (top left) the entropy distribution inside the star at three different epochs for the case with  $\dot{M} = 10 M_\odot \text{ yr}^{-1}$ , where effects of the GR instability is the most prominent. Recall that the polytrope models presume the spatially constant specific entropy in the interior (e.g., Kippenhahn et al. 2012). As seen in Figure 3, however, this is not the case for our accreting stellar models, for which the outer envelope has higher entropy than in the core. Since such an envelope is gravitationally loosely bound, higher total stellar mass is required for the GR instability in the accreting models than in the polytropic model.

Another useful expression for the GR-instability criterion is given by Chandrasekhar (1964) for a polytropic star with the index  $\Gamma (\equiv 1 + 1/n)$ , which states that the star is GR unstable if  $\Gamma < 4/3 + 1.12 (2GM/Rc^2)$ , where  $R$  is the stellar radius. For a highly radiation-dominant state as in SMSs, the adiabatic index in the equation of state can be approximated as  $\Gamma = 4/3 + \beta/6 + O(\beta^2)$ , where  $\beta (\ll 1)$  is the ratio of the gas pressure to total pressure. The criterion for the GR instability can thus be written as

$$\beta/6 < 1.12 (2GM/Rc^2). \quad (3)$$

Note that this condition is obtained for a spatially constant  $\Gamma$ , i.e., for a constant  $\beta$ , which is inversely proportional to the specific entropy  $s$  as  $\beta \simeq 4k_B/\mu s$  for  $\beta \ll 1$ . In our case, this condition should be applied to the isentropic core.

In Figure 3 we show the distributions of  $\beta/6$ ,  $1.12 (2GM_r/rc^2)$ , and  $\mu$  for  $\dot{M} = 10 M_\odot \text{ yr}^{-1}$  at three different epochs with  $M_6 = 0.1, 0.4$  and  $0.8$ . We define the surface of the isentropic core (with mass  $M_s$ ) as the shell where the specific entropy becomes larger than the central value by 1%;  $M_{s,6} = 0.002, 0.016$  and  $0.042$  for  $M_6 = 0.1, 0.4$  and  $0.8$ , respectively. As seen in the figure, as the stellar mass  $M_6$  increases,  $\beta$  becomes smaller while  $M_r/r$  becomes larger at the same mass shell  $M_r$ . Owing to the high value of the specific entropy outside the core,  $\beta$  becomes small in this region with the relation

$\beta \simeq 4k_B/\mu s$ . The mean molecular weight  $\mu$  increases toward the center as the hydrogen burning proceeds. The rise of  $M_r/r$  with the total stellar mass indicates that the more massive star is more concentrated, as in the case for the ordinary primordial stars (e.g., Marigo et al. 2001, 2003). Figure 3 shows that, for  $M_6 = 0.1$ , the condition (3) is not satisfied anywhere and the star is GR-stable. For  $M_6 = 0.4$ , the isentropic core is still GR-stable as condition (3) holds for  $M_{r,6} \geq 0.04$ , only outside the isentropic core  $M_{s,6} = 0.016$ . Finally, when the stellar mass reaches  $M_6 = 0.8$ , equation (3) is satisfied at the surface where  $M_r = M_s$ , and the core begins to collapse. Similarly, we find that the GR instability begins to operate satisfying the condition (3) at some moment for the cases with  $\dot{M} = 0.3$  and  $1.0 M_\odot \text{ yr}^{-1}$ , but never with  $\dot{M} = 0.1 M_\odot \text{ yr}^{-1}$ . From this analysis, we conclude that the GR instability causes the gravitational collapse for the models with  $\dot{M} \gtrsim 0.3 M_\odot \text{ yr}^{-1}$ .

#### 4. DISCUSSIONS AND IMPLICATIONS

We first compare our results with the previous work by Fuller et al. (1986), who study the GR stability of hydrogen-burning stars with fixed masses. They define a star *stable* if the GR instability does not occur during the hydrogen burning stage. The critical stellar mass for the stability  $M_{\text{crit}}$  lies between  $M_6 = 0.1$  and  $0.25$ . However, our calculations show that all the models except for  $\dot{M} = 10 M_\odot \text{ yr}^{-1}$  are “stable” and begin collapsing after the exhaustion of the hydrogen at the center, when the stellar mass is well above  $M_{\text{crit}}$ . Specifically, the star becomes GR-unstable during the helium-burning stage for  $\dot{M} = 0.3 \sim 1.0 M_\odot \text{ yr}^{-1}$  with the final mass  $M_6 = 0.19 \sim 0.35$ . The main difference from Fuller et al. (1986) is that accreting stars that we consider here have a high-entropy envelope. Hence the final masses (including the outer envelope) are larger than  $M_{\text{crit}}$ .

The final stellar masses obtained in this *Letter* should be regarded as upper mass limits for the remnant BHs after the collapse. Chen et al. (2014) argue that energetic supernova explosions occur at the collapse of SMSs in a very narrow mass strip around  $M = 55000 M_\odot$ . Since none of our models end up in this mass range, it is unlikely that such explosions are the final fate of our models. We will provide further results for this issue using a 1D-GR hydrodynamical code in a forthcoming paper. Preliminary results suggest that the BHs with approximately the same mass as the progenitors will be left behind after the collapse.

If the progenitor star is a rapid rotator, some mass ejection or even explosion may occur at the final stellar collapse. An accretion disk can appear around a rotating BH and some outflows or jets can be launched. Shibata et al. (2016), for instance, show by way of a GR hydrodynamics simulation that some portion of the stellar envelope is ejected while most of the stellar matter is drawn into a newborn BH.

We conclude that an accreting protostar at a very large rate of  $\dot{M} = 0.1 - 10 M_\odot \text{ yr}^{-1}$  grows to become a SMS with mass  $1.2 - 8.0 \times 10^5 M_\odot$ . BHs with roughly the same mass will be left as remnants of such SMSs, which might have sown seeds for the formation of supermassive BHs in the early universe.

We thank Masaru Shibata and Koh Takahashi for valuable comments. This work has been supported by Grants-in-Aid for Scientific Research (26400220: HU, 16H05996, 15H00776, 25800102: TH, 25287040: KO,

25287050: NY) from Japan Society for the Promotion of Science and Grant-in-Aid for Scientific Research on Innovative Areas (26104007: HU) from the MEXT in Japan.

## REFERENCES

- Becerra, F., Greif, T. H., Springel, V., & Hernquist, L. E. 2015, *MNRAS*, 446, 2380
- Bromm, V., & Loeb, A. 2003, *ApJ*, 596, 34
- Chandrasekhar, S. 1964, *Physical Review Letters*, 12, 114
- Chen, K.-J., Heger, A., Woosley, S., Almgren, A., Whalen, D. J., & Johnson, J. L. 2014, *ApJ*, 790, 162
- Di Matteo, T., Khandai, N., DeGraf, C., Feng, Y., Croft, R. A. C., Lopez, J., & Springel, V. 2012, *ApJ*, 745, L29
- Fricke, K. J. 1973, *ApJ*, 183, 941
- Fuller, G. M., Woosley, S. E., & Weaver, T. A. 1986, *ApJ*, 307, 675
- Hirano, S., Hosokawa, T., Yoshida, N., Omukai, K., & Yorke, H. W. 2015, *MNRAS*, 448, 568
- Hosokawa, T., Hirano, S., Kuiper, R., Yorke, H. W., Omukai, K., & Yoshida, N. 2016, *ApJ*, 824, 119
- Hosokawa, T., Omukai, K., & Yorke, H. W. 2012, *ApJ*, 756, 93
- Hosokawa, T., Omukai, K., Yoshida, N., & Yorke, H. W. 2011, *Science*, 334, 1250
- Hosokawa, T., Yorke, H. W., Inayoshi, K., Omukai, K., & Yoshida, N. 2013, *ApJ*, 778, 178
- Iben, Jr., I. 1963, *ApJ*, 138, 1090
- Inayoshi, K., Omukai, K., & Tasker, E. 2014, *MNRAS*, 445, L109
- Kippenhahn, R., Weigert, A., & Weiss, A. 2012, *Stellar Structure and Evolution*
- Latif, M. A., Schleicher, D. R. G., Schmidt, W., & Niemeyer, J. 2013, *MNRAS*, 433, 1607
- Marigo, P., Chiosi, C., & Kudritzki, R.-P. 2003, *A&A*, 399, 617
- Marigo, P., Girardi, L., Chiosi, C., & Wood, P. R. 2001, *A&A*, 371, 152
- McKee, C. F., & Tan, J. C. 2008, *ApJ*, 681, 771
- Mortlock, D. J., et al. 2011, *Nature*, 474, 616
- Ohkubo, T., Nomoto, K., Umeda, H., Yoshida, N., & Tsuruta, S. 2009, *ApJ*, 706, 1184
- Omukai, K., & Palla, F. 2003, *ApJ*, 589, 677
- Osaki, Y. 1966, *PASJ*, 18, 384
- Schleicher, D. R. G., Palla, F., Ferrara, A., Galli, D., & Latif, M. 2013, *A&A*, 558, A59
- Shapiro, S. L., & Teukolsky, S. A. 1983, *Black holes, white dwarfs, and neutron stars: The physics of compact objects*
- Shibata, M., Sekiguchi, Y., Uchida, H., & Umeda, H. 2016, *Phys. Rev. D*, 94, 021501
- Stacy, A., Bromm, V., & Lee, A. T. 2016, *MNRAS*, 462, 1307
- Takahashi, K., Umeda, H., & Yoshida, T. 2014, *ApJ*, 794, 40
- Umeda, H., & Nomoto, K. 2002, *ApJ*, 565, 385
- . 2005, *ApJ*, 619, 427
- Umeda, H., Yoshida, N., Nomoto, K., Tsuruta, S., Sasaki, M., & Ohkubo, T. 2009, *J. Cosmology Astropart. Phys.*, 8, 024
- Unno, W. 1971, *PASJ*, 23, 123
- Wu, X.-B., et al. 2015, *Nature*, 518, 512